

Rapid Evolution in the Most Luminous Galaxies During the First 900 Million Years

Rychard J. Bouwens, Garth D. Illingworth

Department of Astronomy, University of California Santa Cruz, 1156 High Street, Santa Cruz, CA 95064, USA

In just three years since the discovery of the first galaxies in the reionization epoch (in the first billion years) 500 galaxies are now known at $z\sim 6$ and exploration is under way for galaxies at $z\sim 7-8$ and higher redshifts.¹⁻³ At $z\sim 6$ we have established very accurately the UV ionizing flux from galaxies, determined the star formation rate, and have accurately measured the rest frame UV luminosity function (LF) to faint limits.³

The bright (massive) end of the LF is quite deficient in galaxies at $z\sim 6$ compared to $z\sim 3$, just 1 billion years later, broadly as expected from hierarchical buildup.³⁻⁶ Yet, the LF and the star formation rate remain very uncertain earlier than 900 million years after recombination due to the great difficulty in obtaining very deep infrared observations. As a result of a growing number of fields with deep optical and infrared (ACS and NICMOS) data from the Hubble Space Telescope (HST), it is finally possible to explore how the LF changes to even earlier times. Here we take advantage of all available deep HST NICMOS data (~ 700 orbits) over the Extended CDF-South and HDF-North GOODS regions with overlapping ACS data to conduct a search for starbursting galaxies at $z\sim 7-8$ using a z_{850} -dropout technique. We only find one object in our most conservative selection and four in a less conservative selection, but expect 10 and 17, respectively, if we assume no-evolution from $z\sim 6$. This is inconsistent with no-evolution at $\geq 99.9\%$ confidence assuming simple Poissonian statistics (and $\geq 99.4\%$ confidence if we include the effects of large-scale structure) and indicates that the volume density of bright ($\sim 0.6-2.5 L_{z=6}^*$) galaxies at $z\sim 7-8$ was much lower than at $z\sim 6$, just 200 million years later. The discovery shows that luminous, massive galaxies are quite deficient 700 million years after recombination, and provides key evidence for hierarchical galaxy buildup at early times.

One particularly effective way of selecting high redshift galaxies is through the well-established “dropout” technique.⁷ This technique allows us to identify high-redshift galaxies through a sharp drop in flux that occurs as a result of absorption by intervening neutral hydrogen.⁸ Applying this technique to study galaxies at redshifts beyond 6 is challenging due to the difficulty in obtaining deep imaging observations at the redder optical or near-infrared wavelengths needed to identify possible sources. With ground-based telescopes, the principal limitation is the high sky backgrounds, which make it difficult for us to detect these extremely faint sources. While near-infrared imaging from space largely overcomes this problem, we are limited by the areal coverage of the available instrumentation. In particular, the HST NICMOS (Near Infrared Camera and Multiobject Spectrograph) instrument – the only near-infrared imaging instrument in space – has a very

small field to view (0.8 arcmin^2), just 7% of the area of the HST ACS (Advanced Camera for Surveys)).⁹ This has made it extremely time consuming to survey large areas of sky for high redshift sources.

NICMOS' small field of view can be partially offset by its many years of operation. There are now $\sim 20 \text{ arcmin}^2$ of deep NICMOS images (J,H ~ 27 -28 AB mag) that overlap with optical HST ACS images of comparable depth (~ 28 -29 AB mag), most of which is available over the two Great Observatories Origins Deep Survey (GOODS) fields. Of these data, perhaps the most well known is the near-infrared data over the Ultra Deep Field (UDF).¹⁰ In some previous work, our group used these data to search for $z > 6.5$ galaxies with a z-dropout criterion and reported a few candidates.¹¹ Note that the z-dropout technique selects sources which have very blue infrared colours, but show a strong flux change ("break") across the z and J bands. This is strongly indicative of star-forming galaxies at $z \sim 7$ -8 (Supplementary Figure 2). Our UDF results were consistent with a slight increase in the volume density of luminous sources from $z \sim 7$ to $z \sim 6$. However, due to uncertainty about possible instrumental problems for some of the candidates and the large uncertainty due to large-scale structure effects, we were not able to draw very strong conclusions about the evolution of the LF over this interval.

In this Letter, we conduct a much more comprehensive search for $z > 6.5$ galaxies by applying a z-dropout selection over a much larger number of fields, using a much improved reduction of the NICMOS data. Not only do we increase the expected number of sources, but we are also able to average over the effects of large scale structure. These search fields are presented in detail in Supplementary Figure 1 and Supplementary Table 1 and include the UDF, UDF NICMOS parallels, HDF-North, and various NICMOS parallels in the GOODS fields. The reductions of the optical (ACS) and near-infrared (NICMOS) imaging data were conducted through standard procedures,¹² and then registered onto the same frame. Object catalogues were generated with SExtractor¹³ based upon all 4σ detections found in a χ^2 image (generated from the J_{110} and H_{160} images), and these catalogues were cleaned of spurious or other marginal detections by requiring objects to be 4.5σ in the H_{160} band (0.3" diameter aperture) and finally PSF-matched.

We then considered two different z-dropout selections on these catalogues. Our first selection was a relatively conservative one that was designed to isolate a robust set of z-dropouts. Our second selection was a little more aggressive and designed to find a larger sample of candidates (albeit less secure). Applying these criteria to our photometric catalogs, only one z-dropout candidate made our conservative selection and four candidate z-dropouts made our less conservative selection. There were two other sources in our search fields that satisfied our selection, but they are very likely to be T-dwarf stars. All four $z \sim 7$ candidates are shown in Figure 1 and their properties listed in Supplementary Table 2. A detailed discussion of our current selection is provided in the Supplementary Information.

What do these z-dropout candidates imply for the evolution of the rest-frame UV LF (the UV LF describes the number density of galaxies versus UV luminosity and can be parametrised by a normalization ϕ^* , characteristic luminosity L^* , and faint end slope α)? To address this, it was useful to compare the current numbers with what we might have expected, if galaxies at $z\sim 7$ were similar to those at $z\sim 6$, just 200 million years later. We can compute this by using our cloning software to artificially redshift the $z\sim 6$ population over the redshift range of our sample, add them to our data, and then repeat the selection.¹⁴⁻
¹⁵ We estimated that we would find 10.1 ± 3.5 z-dropouts using our conservative selection and 17.0 ± 4.9 z-dropouts using our less conservative selection. Since this is substantially more than the 1 and 4 z-dropout candidates found in our conservative and less conservative selections, respectively, this suggests that there has been substantial evolution for galaxies that lie at the bright end of the LF. For simple Poissonian statistics, the present samples are inconsistent with no-evolution at 99.90% and 99.93% confidence, respectively.

To make a proper assessment of the significance of this result, however, we need to account for the effects of galaxy clustering (“large-scale structure”) on this result.³ Modelling the selection volume in our individual fields with a window of depth $\Delta z = 1$ at $z\sim 7-8$ and bias of 7, we estimate the field-to-field variance to be $\sim 41\%$ and $\sim 49\%$ for our ~ 5 arcmin² fields and 0.8 arcmin² fields, respectively.¹⁶⁻¹⁷ Including the effect of large-scale structure increases the uncertainties on our expected numbers, i.e., $10.1_{-5.0}^{+3.1}$ sources with our conservative search and $17.0_{-7.2}^{+4.7}$ sources for our less-conservative search. Again, this is inconsistent with no-evolution at 99.5% and 99.4% confidence, respectively, and suggested that there has been a dramatic drop in the overall prevalence of luminous galaxies over this interval. We estimate that the number density of luminous galaxies at $z\sim 7.4$ is just $0.10_{-0.07}^{+0.19} \times$ that at $z\sim 6$ for our conservative search and $0.24_{-0.12}^{+0.20} \times$ the $z\sim 6$ value for our less-conservative selection. The two determinations here are consistent within the errors and suggest that our basic result here is robust. For simplicity, we will use statistics from our more rigorous, conservative search for the remainder of this paper.

What does this deficit of luminous star-forming objects at $z\sim 7$ tell us about evolution of the UV LF? This deficit could be due to a change in the overall number density of galaxies or due to a change in luminosity of the brightest objects. Perhaps the simplest and most natural explanation though is through an evolution of the characteristic luminosity. Since it is already well established that the characteristic luminosity of galaxies brightens significantly over the interval $z\sim 6$ to $z\sim 3$ (Figure 2),^{3,5} it seems reasonable to imagine that this trend continues from $z\sim 7$ to $z\sim 6$. A relevant question to ask is how much fainter the characteristic luminosity at $z\sim 7$ would need to be to reproduce the observed decline. There are two obvious ways to model this change: (1) a simple scenario where we vary L^* while keeping the normalization $\phi^* = 0.002$ Mpc⁻³ and faint-end slope $\alpha = -1.73$ fixed at the $z\sim 6$ values and (2) a scenario where we vary L^* while keeping the product of ϕ^* and L^* fixed (and α fixed) to maintain a constant luminosity density at $z\geq 6$. The latter scenario is motivated by a number of recent results at high redshift, which suggest that the rest-frame UV luminosity density – and the total star formation rate density -- shows very mild

evolution.^{3,18} These latter observations include the high stellar masses found in many $z\sim 6$ systems and large optical depths measured by *WMAP* ($\tau = 0.09\pm 0.03$), both of which suggest substantial high-redshift ($z>6$) star formation.¹⁹⁻²² For the above scenarios, we can evaluate the evolution in the characteristic luminosity needed to produce the factor of ~ 10 deficit in luminous galaxies at $z\sim 7.4$ by repeating the Monte-Carlo simulations described above. The end result is that we find that the characteristic luminosity at $z\sim 7.4$ in the rest-frame UV ($\sim 1900 \text{ \AA}$) must be 1.1 ± 0.4 mag fainter than $z\sim 6$ to reproduce the observed result for our first set of assumptions and 1.5 ± 0.4 mag fainter for our second (see Figure 2). In both cases, the evolution is fairly dramatic and suggests that most galaxies at $z\sim 7$ are much fainter than our survey limits.

In summary, we have demonstrated that there is a substantial deficit of luminous (and likely massive star-forming) galaxies at $z\sim 7$ relative to $z\sim 6$, just 200 million years later. The simplest explanation for this deficit is that the universe is simply too young to have built up many luminous systems, and that the majority of galaxies at $z\sim 7.4$ have luminosities much fainter than an AB mag ~ -19.7 , the approximate magnitude limit of this search. To test this hypothesis, we will need to extend current high redshift searches significantly deeper to probe this potentially dominant population of star-forming objects. Though there are a few ongoing HST programs that should provide further gains at these levels, significantly better insights will only come from the much deeper probes made possible by HST Wide Field Camera 3 IR channel within the next couple of years, and then ultimately with the powerful imaging capability of James Webb Space Telescope.

1. Becker, *et al.* Evidence for Reionization at $z\sim 6$: Detection of a Gunn-Peterson Trough in a $z=6.28$ Quasar, *Astronom. J.*, **122**, 2850-2857 (2001).
2. Fan, X., *et al.* Evolution of the Ionizing Background and the Epoch of Reionization from the Spectra of $z\sim 6$ Quasars, *Astronom. J.*, **123**, 1247-1257 (2002).
3. Bouwens, R.J., Illingworth, G.D., Blakeslee, J.P., & Franx, M. Galaxies at $z\sim 6$: The UV Luminosity Function and Luminosity Density from 506 UDF, UDF-Ps, and GOODS i-dropouts, *Astrophys. J.*, *in press* (2006).
4. Stanway, E.R., Bunker, A.J., & McMahon, R.G. Lyman break galaxies and the star formation rate of the Universe at $z\sim 6$, *Month. Not. R. Astron. Soc.*, **342**, 439-445 (2003).
5. Dickinson, M., *et al.* Color-selected Galaxies at $z\sim 6$ in the Great Observatories Origins Deep Survey, *Astrophys. J. Lett.*, **600**, 99-102 (2004).
6. Shimasaku, K., Ouchi, M., Furusawa, H., Yoshida, H., Kashikawa, N. Okamura, S., Number Density of Bright Lyman-Break Galaxies at $z\sim 6$ in the Subaru Deep Field, *Public. Astro. Soc. Japan*, **57**, 447-458 (2005).
7. Steidel, C.C., Giavalisco, M., Pettini, M., Dickinson, M., & Adelberger, K.L. Spectroscopic Confirmation of a Population of Normal Star-forming Galaxies at Redshifts $Z > 3$, *Astrophys. J. Lett.*, **462**, 17-20 (1996).

8. Madau, P. Radiative transfer in a clumpy universe: The colors of high-redshift galaxies, *Astrophys. J.*, **441**, 18-27 (1995).
9. Skinner, C.J., *et al.* On-orbit properties of the NICMOS detectors on HST, *Proc. SPIE* **3354**, 2-13 (1998).
10. Thompson, R.I., *et al.* The Near-Infrared Camera and Multi-Object Spectrometer Ultra Deep Field: Observations, Data Reduction, and Galaxy Photometry, *Astron. J.*, **130**, 1-12 (2005).
11. Bouwens, R.J., *et al.* Galaxies at $z \sim 7-8$: z_{850} -Dropouts in the Hubble Ultra Deep Field, *Astrophys. J. Lett.*, **616**, 79-82 (2004).
12. Blakeslee, J.P., Anderson, K.R., Meurer, G.R., Benítez, N., Magee, D. An Automatic Image Reduction Pipeline for the Advanced Camera for Surveys, *Astronomical Data Analysis Software and Systems XII ASP Conference Series*, **295**, 257-260 (2003).
13. Bertin, E. & Arnouts, S. SExtractor: Software for source extraction, *Astron. Astrophys. Suppl.*, **117**, 393-404 (1996).
14. Bouwens, R.J., Broadhurst, T.J., Silk, J. Cloning Hubble Deep Fields. I. A Model-independent Measurement of Galaxy Evolution, *Astrophys. J.* **506**, 557-578 (1998).
15. Bouwens, R.J., Broadhurst, T.J., Illingworth, G.D. (2003). Cloning Dropouts: Implications for Galaxy Evolution at High Redshift, *Astrophys. J.* **593**, 640-660 (2003).
16. Mo, H.J., & White, S.D.M. An analytic model for the spatial clustering of dark matter haloes, *Month. Not. R. Astron. Soc.*, **282**, 347-361 (1996).
17. Somerville, R.S., *et al.* Cosmic Variance in the Great Observatories Origins Deep Survey, *Astrophys. J. Lett.*, **600**, 171-174 (2004).
18. Giavalisco, M., *et al.* The Rest-Frame Ultraviolet Luminosity Density of Star-forming Galaxies at Redshifts $z > 3.5$, *Astrophys. J. Lett.*, **600**, 103-106 (2004).
19. Eyles, L., *et al.* Spitzer imaging of i'-drop galaxies: old stars at $z \sim 6$, *Month. Not. R. Astron. Soc.*, **364**, 443-454 (2005).
20. Yan, H., *et al.* Rest-frame Ultraviolet-to-Optical Properties of Galaxies at $z \sim 6$ and 5 in the Hubble Ultra Deep Field: from Hubble to Spitzer, *Astrophys. J.*, **634**, 109-127 (2005).
21. Yan, H.J., Dickinson, M., Giavalisco, M., Stern, D., Eisenhardt, P.R., Ferguson, H.C., The Stellar Masses and Star Formation Histories of Galaxies at $z \sim 6$: Constraints from Spitzer Observations in the Great Observatories Origins Deep Survey, *Astrophys. J.*, in press (2006).
22. Spergel, D., *et al.* Wilkinson Microwave Anisotropy Probe (WMAP) Three Year Results: Implications for Cosmology, *Astrophys. J.*, submitted (2006).
23. Labbe, I., Bouwens, R.J., Illingworth, G.D., Franx, M. Confirmation of z-dropout galaxies in the HUDF with Spitzer IRAC imaging: Stellar Masses and Ages, *Astrophys. J. Lett.*, submitted (2006).

24. Steidel, C.C., Adelberger, K.L., Giavalisco, M., Dickinson, M., and Pettini, M. Lyman-Break Galaxies at $z \sim 4$ and the Evolution of the Ultraviolet Luminosity Density at High Redshift, *Astrophys. J.*, **519**, 1-17 (1999).
25. Schiminovich, D., *et al.* The GALEX-VVDS Measurement of the Evolution of the Far-Ultraviolet Luminosity Density and the Cosmic Star Formation Rate, *Astrophys. J. Lett.*, **619**, 47-50 (2005).
26. Madau, P., Pozzetti, L. & Dickinson, M. The Star Formation History of Field Galaxies, *Astrophys. J.*, **498**, 106-116 (1998).
27. Stanway, E.R., McMahon, R.G., & Bunker, A.J. Near-infrared properties of i-drop galaxies in the Hubble Ultra Deep Field, *Month. Not. R. Astron. Soc.*, **359**, 1184-1192 (2005).
28. Knapp, G.R., *et al.* Near-Infrared Photometry and Spectroscopy of L and T Dwarfs: The Effects of Temperature, Clouds, and Gravity, *Astron. J.* **127**, 3553-3578 (2004).
29. Ferguson, H.C., *et al.* The Size Evolution of High-Redshift Galaxies, *Astrophys. J. Lett.*, **600**, 107-1110 (2004).
30. Kron, R.G. Photometry of a complete sample of faint galaxies, *Astrophys. J. Suppl.*, **43**, 305-325 (1980).

Acknowledgements: We are immensely grateful to Louis Bergeron, Susan Kassin, Daniel Magee, Massimo Stiavelli, and Rodger Thompson for their help in reducing the NICMOS data used here for $z > 6.5$ searches. We also acknowledge Marijn Franx for a very careful and critical read of this manuscript, Sangeeta Malhotra for making the NICMOS parallels to her PEARS program public early, and Ivo Labbe for help with the interpretation of the IRAC data.

Correspondence and requests for materials should be addressed to R.B. (e-mail: bouwens@ucolick.org)

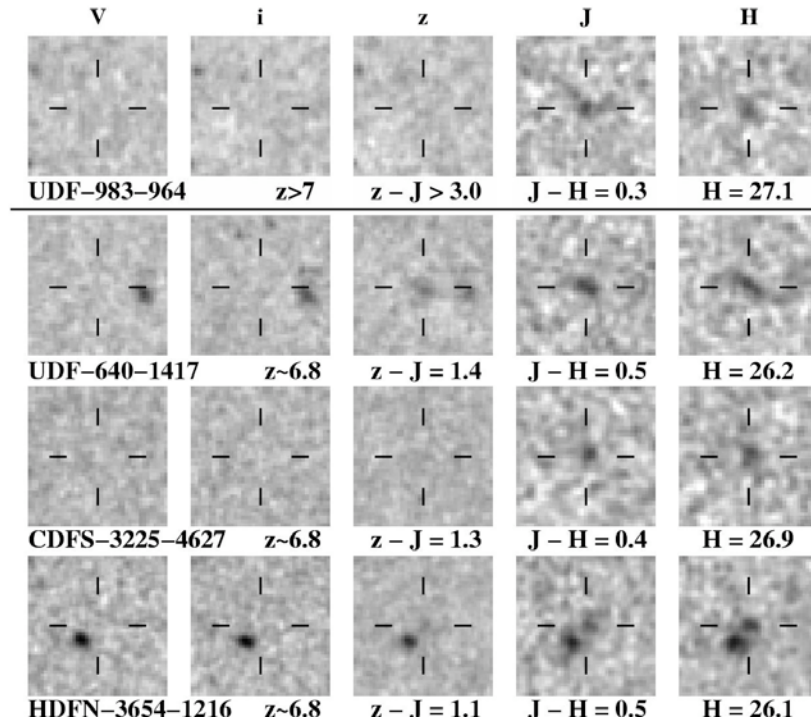


Figure 1. Optical and near-infrared images of four candidate galaxies at $z \sim 7$. The uppermost candidate is the only object satisfying our most conservative z -dropout criterion ($Z_{850} - J_{110} > 1.3$, $Z_{850} - J_{110} > 1.3 + 0.4(J_{110} - H_{160})$, $J_{110} - H_{160} < 1.2$, undetected [$< 2\sigma$] in the V_{606} and i_{775} bands). This object is undetected ($< 2\sigma$) in the extremely deep optical BViz data available in the HUDF, has a $Z_{850} - J_{110}$ colour redder than 3.0 AB mag (1σ), and $J_{110} - H_{160}$ colour of 0.3. It also shows a significant 5σ detection in the InfraRed Array Channel (IRAC) 3.6μ and 4.5μ coverage we have from the Spitzer Space Telescope,²³ with optical-IR colours very similar to dropouts found at $z \sim 6$.¹⁹⁻²¹ While this object lacks spectroscopic confirmation (and will likely continue to do so – because it is so faint), it seems extremely probable that it is at $z \sim 7$. It had previously been reported as a z -dropout candidate in the HUDF.¹¹ The lower three candidates satisfy our less conservative z -dropout criterion ($Z_{850} - J_{110} > 0.8$, $Z_{850} - J_{110} > 0.8 + 0.4(J_{110} - H_{160})$, $J_{110} - H_{160} < 1.2$, undetected [$< 2\sigma$] in the V_{606} and i_{775} bands). Though each of these sources appear consistent with being just at the low-redshift edge of the selection ($z \sim 6.8$), the optical imaging available for two of these sources (CDFS-3225-4627 and HDFN-3654-1216) is not deep enough to completely rule out their being low-redshift sources (or T-dwarf stars in the case of CDFS-3225-4627). All z -dropout candidates considered here were detected at $> 4\sigma$ and $> 4.5\sigma$ in the J and H bands, respectively, and were found in NICMOS data with at least 7 individual exposures. The V, i, z, J, and H images shown here correspond to the ACS F606W, ACS F775W, ACS F850LP, NICMOS F110W, and NICMOS F160W filters, respectively, with central wavelengths of 591, 776, 944, 1119, and 1604 nm, respectively. Each cutout is $3.5'' \times 3.5''$ in size.

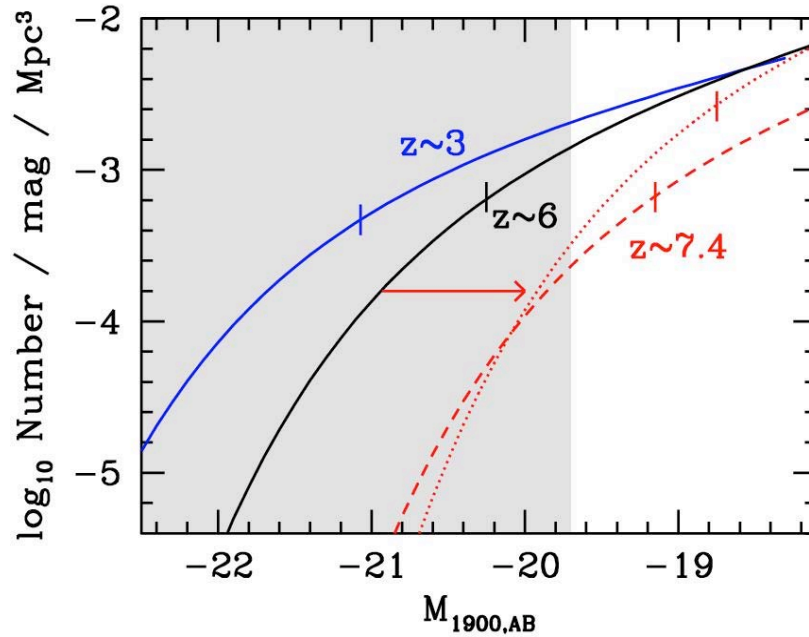


Figure 2. Two possible luminosity functions (LFs) at $z\sim 7.4$ that are consistent with the surface density of $z\sim 7$ galaxies (z-dropouts) found over our search fields and compared with the $z\sim 6$ and $z\sim 3$ LFs.^{3,24} The characteristic luminosity for each LF is indicated on the figure with a short vertical line. The grey region shows the approximate flux range of the current z-dropout study. The rest-frame UV LFs brightens considerably from $z\sim 6$ to $z\sim 3$, and it seems reasonable to imagine that this trend continues from even earlier times (i.e., from $z\sim 7.4$ to $z\sim 6$). The first LF (dashed line) was obtained by requiring the $z\sim 7.4$ LF to have the same normalization ϕ^* and faint-end slope α as the LF at $z\sim 6$ (solid black line),³ but changing the characteristic luminosity L^* to match the observed surface density of $z\sim 7$ galaxies. The second LF (dotted line) was obtained by requiring the product of ϕ^* and L^* to be a constant (to maintain an approximately constant luminosity density), fixing α to the $z\sim 6$ value (-1.73), but changing the characteristic luminosity L^* to match the observed surface density of $z\sim 7$ galaxies. The characteristic luminosity which best fits our search results is 1.1 ± 0.4 mag fainter than the $z\sim 6$ value for the first LF and 1.5 ± 0.4 mag fainter for the second LF (equivalent to $H_{160,AB}$ -band magnitudes of 28.0 ± 0.4 AB mag and 28.4 ± 0.4 AB mag, respectively). The “concordance” cosmology ($\Omega_m=0.3, \Omega_\Lambda=0.7, H=70$ km/s/Mpc³) is assumed.

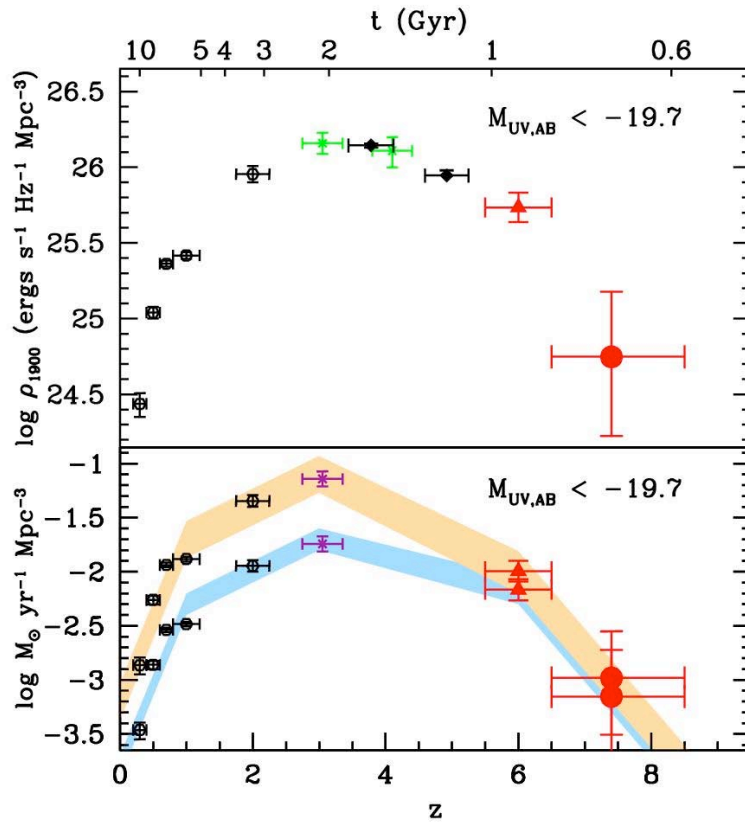


Figure 3. The luminosity density and star formation rate density of the universe. The top panel shows the rest-frame UV luminosity density from $z \sim 0$ to $z \sim 7.4$. Because of the flux limits of the current z -dropout searches, we only plot the luminosity densities down to a flux limit of -19.7 AB mag (which is equivalent to 0.6 times $L_{z=6}^*$: the characteristic luminosity at $z=6$).³ The new determination is shown as a large filled circle at $z \sim 7.4$ (with 1σ errors that include both Poissonian and large-scale structure uncertainties) and compared with determinations at $z \sim 0-2$ (open squares),²⁵ $z \sim 3$ (green crosses),²⁴ $z \sim 4-5$ (black diamonds),¹⁸ and $z \sim 6$ (red triangle).³ The luminosity density shows an abrupt increase from $z \sim 7.4$ to $z \sim 6$, indicating that there has been a rapid buildup in luminous ($>0.6 L_{z=6}^*$) galaxies over this range in redshift – which corresponds to a period of just 0.2 Gyr. The bottom panel presents the star formation history of the universe shown with and without a correction for dust extinction (upper and lower points, respectively). This star formation history is derived from the UV luminosity densities assuming a Salpeter IMF, which extends from $0.1 M_{\text{sol}}$ to $100 M_{\text{sol}}$.²⁶ To account for the apparent evolution in the UV colours and thus dust properties of high redshift galaxies,^{2,21,27} we apply more minimal (~ 0.4 mag) dust corrections at $z > 5$, but revert to more standard values (~ 1.4 mag) at $z \leq 3$.²⁵ The “concordance” cosmology ($\Omega_m=0.3$, $\Omega_\Lambda=0.7$, $H=70$ km/s/Mpc³) is assumed.

Supplementary Information: Rapid Evolution in the Most Luminous Galaxies During the First 900 Million Years, Rychard J. Bouwens, Garth D. Illingworth, Department of Astronomy, University of California Santa Cruz, 1156 High Street, Santa Cruz, CA 95064, USA

Reductions of the Optical and Infrared (ACS/NICMOS) Data

In order to maximize the overall uniformity of the NICMOS data set, we rereduced the majority of the data using our recently implemented NICMOS pipeline. All exposures were subjected to the standard NICMOS processing procedures: flat fielding, bias and pedestal correction, cosmic ray rejection, bad pixel masking, treatment for SAA passage, and treatment for the “Mr. Staypuft” anomaly (which produces artificial sources 128 pixels from bright sources).⁹ The individual exposures were then aligned and stacked, rejecting pixels more than 4σ outside the median. The only NICMOS data we did not re-reduce were those from the HDF-North, which were taken under very different operating conditions (prior to the refurbishment of the NICMOS camera in 2002, which changed its operating characteristics very significantly.)

For the ACS data, we made use of the public UDF reduction and our own reduction of the ACS GOODS data, which included the ACS data from the SNe search program (for a total of >9 orbits of z_{850} band data at each position in the GOODS mosaic).³ For the two UDF NICMOS parallel fields (for which the initial public release was not optimal), we reduced the ACS data with the ACS GTO pipeline “apsis” which handled the alignment, cosmic-ray rejection, and drizzling of the data onto a final output frame.¹²

Selection Criteria for both of our z-dropout Samples

For our primary, most conservative z-dropout selection, we required $(z_{850}-J_{110})>1.3$, $(J_{110}-H_{160})<1.2$, the candidates to be undetected ($<2\sigma$) in the $V_{606i775}$ imaging, and finally that $z_{850}-J_{110} > 1.3 + 0.4(J_{110}-H_{160})$. For the typical blue (UV continuum slope $\beta \sim -2$) starburst galaxy at $z>5$, this selection probes objects over the range $z\sim 6.8-8.0$. We chose a relatively stringent z-J cut to make our primary selection as clean as possible and largely exclude the region occupied by T-dwarfs (see Supplementary Figure 2).²⁸ Our $(J_{110}-H_{160})$ colour criterion was set to allow a good discrimination against redder galaxies at $z\sim 1-2$, but still include bluer high-redshift objects out to redshifts as high as $z\sim 8$. As an alternative to our primary selection, we also considered a selection with a weaker requirement on the $z_{850}-J_{110}$ colour to find candidate galaxies at slightly lower redshifts $z\sim 6.5$ and to test the robustness of the results we derived from our primary selection. The criteria for this less-

conservative selection were $z_{850}-J_{110} > 0.8$, $z_{850}-J_{110} > 0.8 + 0.4(J_{110}-H_{160})$, $J_{110}-H_{160} < 1.2$, with no detection ($< 2\sigma$) in the V_{606} and i_{775} bands. Note that in computing the z - J colour for both of our z -dropout selections, we set the z -band flux to its 1σ upper limit in case of a non-detection. Both criteria are illustrated on Supplementary Figure 2 with the photometric sample over-plotted.

Conservative Selection

Only two objects from our search fields satisfied our most conservative selection criteria. The first object has a ($z_{850}-J_{110}$) break greater than 3.0 (1σ) and a ($J_{110}-H_{160}$) colour of 0.3, indicative of a very blue UV continuum slope $\beta \sim -2.5$. The $H_{160,AB}$ magnitude is 27.1, corresponding to a UV luminosity of -20.0 AB mag. This object shows a clear (5σ) detection in the Spitzer Space Telescope IRAC (InfraRed Array Camera) 3.6μ and 4.5μ data,²³ with optical-IR colours consistent with i -dropouts found in the GOODS/UDF data.¹⁹⁻²¹ Since its z - J break is > 3.0 (1σ), it is too red to be a low-mass star, but far too blue (in its J - H colour) to be a low-redshift galaxy. Together these data indicate a very robust detection of a star forming galaxy at $z > 7.3$. This object had previously been reported as a z -dropout candidate in the UDF (UDF-983-964).¹¹ The second object in our selection (03:32:25.10, $-27:46:35.6$) has a z - J colour equal to 2.0, an H_{160} -band magnitude of 24.5, an J - H colour of 0.0, and is unresolved in the z_{850} band. It is therefore almost certainly a T-dwarf (see Supplementary Figure 2).

Less Conservative Selection

There were four additional objects in our alternate selection, not present in our conservative selection. The first of these objects is a well-known high- z redshift candidate from the UDF (UDF-640-1417),¹¹ and it just missed our earlier UDF z -dropout selection.¹¹ The second object from this selection (12:37:34.26, 62:18:31.4) again appears to be a T dwarf, being completely unresolved in the z_{850} band. The nature of the two remaining objects from this selection (HDFN-3654-1216 and CDFS-3225-4627) was less easy to establish. Though they appear consistent with having redshifts just above $z \sim 6.5$, we could not completely rule out their being lower redshift sources, or a T-dwarf in the case of CDFS-3225-4627. Of particular concern was HDFN-3654-1216, which together with its close neighbor, is somewhat bright in the public Spitzer IRAC data over the HDF North. The detection in the 3.6μ channel ($m_{3.6\mu,AB} \sim 24$) suggests that it may be a low-redshift interloper.

Comparison with our previous UDF z-dropout selection

It is useful to compare our current z-dropout candidates from the UDF with those from our previous search.¹¹ In that work, we reported 5 possible z-dropout *candidates* over the UDF, but noted that there were concerns about possible contamination and instrumental effects. The most significant result in our previous paper was an upper limit. Using a new reduction of the NICMOS data over the UDF with a more conservative selection criterion, we find that only one of our original five candidates makes it into our present selection. Of the four candidates which miss our conservative selection, two (UDF-491-880 and UDF-818-886) are electronic ghosts of bright stars in the UDF (“the Mr. Staypuft effect”).⁹ Since the electronic ghosts of bright sources are now explicitly modelled and removed, such sources are not a concern for the current selection. The other two candidates (UDF-387-1125 and UDF-825-950), though evident in our reductions at lower significance, did not meet the more stringent selection requirements made here for the present samples.

Expected Number of z-dropouts Assuming No-Evolution From z~6

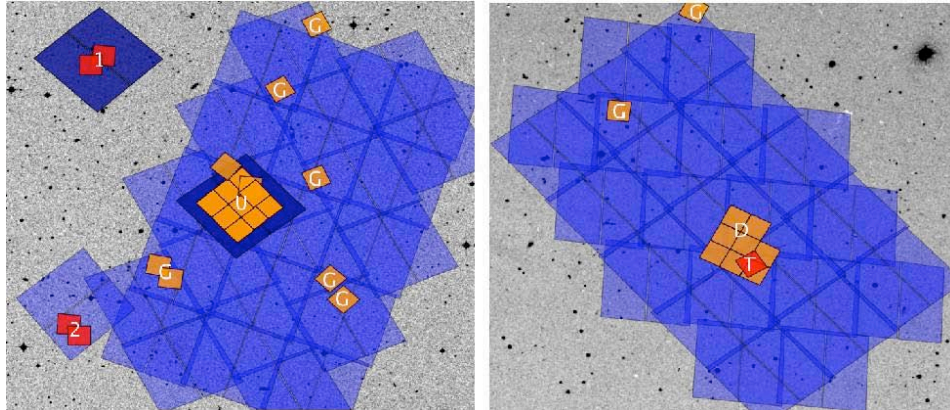
We ran a series of Monte-Carlo simulations using our well-established cloning software, which enables us to generate realistic simulations of galaxies in the high-redshift universe.^{14,15} Input catalogues for the z~6-10 universe were generated on the basis of the z~6 LF⁴ and images generated by artificially redshifting similar luminosity B-dropouts (z~4) to the catalogue redshift, scaling the sizes as $(1+z)^{-1.1}$ (while keeping the luminosity fixed) to account for the expected size evolution and preserving the pixel-by-pixel morphologies.^{3,29} The projected sample was assumed to have the same color distribution as that inferred at z~6 (i.e., a mean UV continuum slope β of -2.0 and 1σ scatter of 0.5).^{3,20,27} The simulated images were then added to the ACS/NICMOS images which made up our search fields, and our selection procedure repeated. This latter step was particularly valuable given the rather heterogeneous nature of our search fields, with significant variations in the S/N of the optical and infrared data. The above simulations were repeated more than 20 times on each search field to minimize dependencies upon any particular realization. These no-evolution simulations showed that we should find $\sim 10.1 \pm 3.2$ galaxies over our search fields for our conservative z-dropout selection. 17.0 ± 4.1 galaxies were predicted for the less-conservative selection criteria, again if there was no evolution in the UV LF from z~7 to z~6. Incorporating the uncertainties in the z~6 LF which result from large-scale structure and small number statistics (estimated to make the overall normalization of the z~6 LF uncertain at the $\sim 16\%$ level), the no-evolution predictions for our two selections become $\sim 10.1 \pm 3.5$ and 17.0 ± 4.9 , respectively. The mean redshift for our z₈₅₀-dropout selection was z~7.4 in the simulations, but this selection ranged from z~6.5 to z~8.5. Most of the z₈₅₀-dropouts recovered in the simulations had H_{160,AB} magnitudes ranging from 26.0 to 27.5, suggesting that the current search was most effective at probing absolute magnitudes between -19.7 and -21.2 AB mag (or 0.6 - 2.5 $L_{z=6}^*$).

Field-to-Field Variations

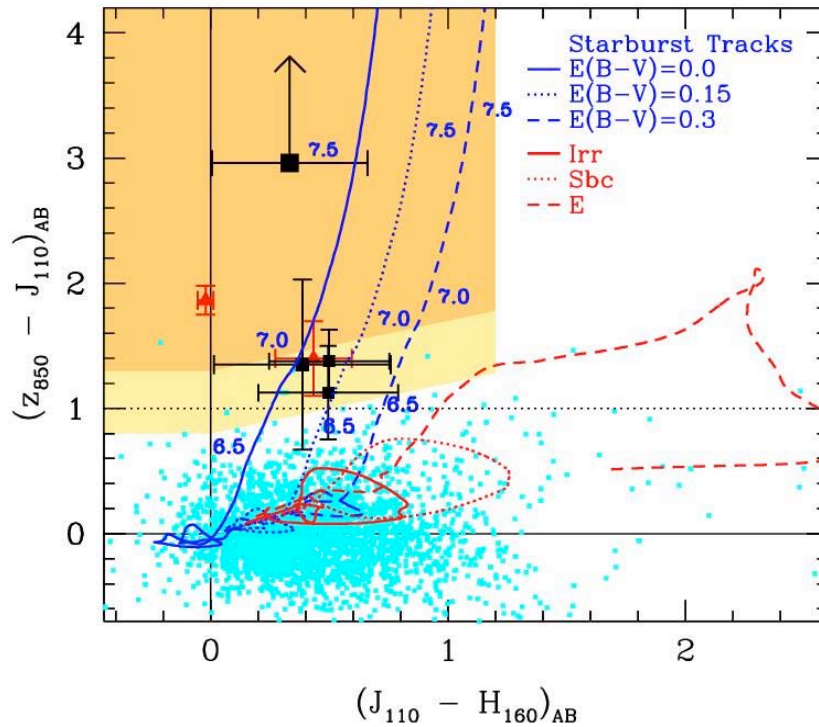
Current theories for the growth of structure allow us to estimate the impact of the clustering provided we have a good estimate of the bias, which provides a link between the observed galaxies and the underlying fluctuations in the mass. It has become conventional to calculate the bias for a population by considering the number density of a population, converting this to a mass scale and then calculating the equivalent bias.¹⁶ For the current search which probes to volume densities of $\sim 10^{-4} \text{ Mpc}^{-3}$, this corresponds to a bias of 7.^{16,17} Then, assuming a pencil-beam geometry and selection window of width $\Delta z = 1$ at $z \sim 7-8$, we estimate the RMS variance in the number density of z_{850} -dropouts in each of our search fields. This variance is 49% for single 0.8 arcmin^2 Near Infrared Camera 3 (NIC3) pointings and 41% for larger $\sim 5 \text{ arcmin}^2$ search fields like the UDF or HDF North NICMOS mosaics. Since the entire CDF-S or HDF-N GOODS field (150 arcmin^2) has an estimated RMS variance of $\sim 24\%$, approximately 30% of the variance in our individual NICMOS fields is coherent across the larger field. Field-to-field variance is modeled using a log-normal distribution.

Star Formation Rate Density

The current measure of the rest-frame UV LF at $z \sim 7.4$ can be used to estimate of the rest-frame UV luminosity density and star formation rate densities to the approximate magnitude limit of the probe ($M_{\text{UV,AB}} = -19.7$ or $0.6 L_{z=6}^*$). Using the luminosity density at $z \sim 6$ down to this limit and multiplying by the evolutionary factor $0.10_{-0.07}^{+0.19} \times$ derived from our most conservative selection, we find a rest-frame (1900 \AA) UV luminosity density of $5.4_{-3.8}^{+9.2} \times 10^{24} \text{ erg/cm}^2/\text{s}/\text{Mpc}^3$. For a Salpeter initial mass function with an assumed mass range $0.1 - 100 M_{\text{sol}}$, this luminosity density translates into an unextincted star formation rate (SFR) density of $6.7_{-4.8}^{+11.2} \times 10^{-4} M_{\odot} \text{ Mpc}^{-3} \text{ yr}^{-1}$.²⁶ We plot the current determination in Figure 3 and compare it against previous measures of the SFR density over the range $0 \leq z \leq 7.4$.^{3,18,24,25} There is a clear, almost precipitous rise in the UV luminosity density from $z \sim 7.4$ to $z \sim 6$. However, it is important to remember that this is just the evolution of the SFR density evaluated down to a relatively bright flux limit (-19.7 AB mag or $0.6 L_{z=6}^*$). Since galaxies in general are likely to be less massive (and hence less luminous) at $z \sim 7.4$ than at $z \sim 6$, it seems probable that a substantial fraction of the total star formation at $z \sim 7.4$ is below this limit, and that the evolution in the total SFR density is much shallower than shown in Figure 3.



Supplementary Figure 1. Search fields used in this Letter to find $z\sim 7-8$ z -dropouts. The left and right panels (18 arcmin on a side) show the CDF-S and HDF-N GOODS fields, respectively. Our NICMOS search areas are labeled (“U”=“UDF”, “1”=“UDF NICPAR1”, “2”=“UDF NICPAR2”, “D”=“Dickinson”, “T”=“Thompson”, and “G”=“GOODS”) to allow easy identification with the fields listed in Supplementary Table 1. These search areas are colour-coded according to their depth to give our readers a sense for the available data. The orange and red regions correspond to NICMOS pointings with 5σ depths of >27 and >28 , respectively, in J_{110} and H_{160} . The dark blue regions show the ultra deep ACS data available over the UDF and UDF NICMOS parallel field #1. The light blue regions show the area covered by the deep *Viz* ACS data over the GOODS fields and UDF NICMOS parallel field #2.



Supplementary Figure 2. $(z_{850} - J_{110})_{AB} / (J_{110} - H_{160})_{AB}$ colour-colour diagram used for selecting our high-redshift z -dropout sample. The selection window for our primary z -dropout sample is shown with the orange shading and only includes one plausible $z > 7$ candidate (shown as large black square with an arrow showing the 1σ lower limit on its $z_{850} - J_{110}$ colour). The selection window for our other z -dropout samples is shown with the light orange shading and includes three plausible $z > 6.5$ candidates (shown as the smaller black squares with 1σ errors). Sources detected ($>2\sigma$) in the HST ACS V_{606} or i_{775} band images are plotted in cyan. The red triangles mark the position of two probable T-dwarfs. The objects shown here are from the UDF, HDF-North, the UDF NICMOS Parallels, and other NICMOS parallels over the GOODS field (Supplementary Table 1 and Supplementary Figure 1). Colour-colour tracks for 10^8 yr constant star formation models with different amounts of dust extinction ($E(B-V)$) are overplotted (blue lines) to indicate the likely position of $z > 6.5$ candidates. Similar tracks are also included for several low-redshift galaxy spectral templates (red lines).²⁸ Lower mass stars are expected to have $(z_{850} - J_{110})_{AB}$ colours of $\sim 1.0 - 1.8$ and $(J_{110} - H_{160})_{AB}$ colours of $\sim 0.0 - 1.3$, and so contamination is a concern for our less conservative selection.

Supplementary Table 1. z-dropout search fields

Field	Area (arcmin ²)	z ₈₅₀ Depth	J ₁₁₀ Depth	H ₁₆₀ Depth
UDF	6.5	29.0	27.7	27.5
UDF NICPAR 1	1.3	28.6	28.7	28.5
UDF NICPAR 2	1.3	27.5	28.7	28.5
GOODS	4.9	27.5	27.2	27.0
HDF-North Thompson	0.8	27.8	28.0	28.1
HDF-North Dickinson	4.0	27.8	27.0	27.0

The depths quoted are the typical 5σ depths in $0.6''$ -diameter aperture in the z₈₅₀, J₁₁₀, and H₁₆₀ bands over those areas. Here the GOODS search fields include all areas over the ACS GOODS fields (excluding the UDF or HDF-North) with deep NICMOS observations. Supplementary Figure 1 shows the position and general layout of the above fields. The FWHM of the PSF for the NIC3 J and H data is $\sim 0.35''$, except for the case of the HDF-North data where it was $\sim 0.25''$. Note that for the HDF-North WFPC2 field where coverage is available from both the Thompson and Dickinson programs (Supplementary Figure 1), we used the deeper HDF-N Thompson data for z-dropout searches over that 0.8 arcmin² field and the Dickinson data otherwise. We have quoted a correspondingly smaller area for the HDF-N Dickinson mosaic to account for the overlap. Also note that for the few regions where there is a mismatch between the depths of our optical and infrared data (most notably in the case of the UDF NICPAR2), our z-dropout search is limited by the depth of the shallower ACS data.

Supplementary Table 2. z-dropout ($z > 6.5$) candidates

Object ID	Right Ascension	Declination	$H_{160,AB}$	$z_{850}-J_{110}$	$J_{110}-H_{160}$	Ref
UDF-983-964	03:32:38.79	-27:47:07.1	27.0 ± 0.2	>3.0	0.3 ± 0.3	[11]
UDF-640-1417	03:32:42.56	-27:46:56.6	26.2 ± 0.1	1.4 ± 0.2	0.5 ± 0.2	[11]
CDFS-3225-4627	03:32:25.22	-27:46:26.6	26.9 ± 0.2	1.3 ± 0.6	0.4 ± 0.4	----
HDFN-3654-1216	12:36:54.12	62:12:16.2	26.1 ± 0.1	1.1 ± 0.4	0.5 ± 0.3	----

All coordinates are for the J2000 equinox. Total magnitudes here are quoted in the H_{160} band and were measured in large apertures (with typical diameters of $1.1''$).³⁰ Colours were measured within a small aperture (with typical diameters of $0.5''$). The uppermost object in this table (UDF-983-964) is the only source in our most conservative z-dropout selection ($z_{850}-J_{110} > 1.3$, $z_{850}-J_{110} > 1.3 + 0.4(J_{110}-H_{160})$, $J_{110}-H_{160} < 1.2$, undetected [$<2\sigma$] in V_{606} and i_{775} bands). All four sources in this table are in our less conservative z-dropout selection ($z_{850}-J_{110} > 0.8$, $z_{850}-J_{110} > 0.8 + 0.4(J_{110}-H_{160})$, $J_{110}-H_{160} < 1.2$, undetected [$<2\sigma$] in V_{606} and i_{775} bands).